AGU PUBLICATIONS

Radio Science

RESEARCH ARTICLE
10.1002/2014RS005418

Special Section:
Beacon Satellite Symposium 2013

# Observed high-latitude GNSS disturbances during a less-than-minor geomagnetic storm

**Y. L. Andalsvik[1] and K. S. Jacobsen[1]**

[1] Norwegian Mapping Authority, Hønefoss, Norway

**Abstract** This paper presents the effects of a weak geomagnetic storm event on 17 January 2013. While the *Kp* index reached a maximum of only 4, this event still caused severe disturbances for Global Navigation Satellite Systems (GNSS)-based positioning services at high latitudes. We present data from the Norwegian Mapping Authority's Real Time Ionospheric Monitor, based on a dense network of geodetic receivers and scintillation indices from scintillation receivers located in Norway. In northern parts of Norway, the centimeter positioning service was severely disturbed for hours. Service-monitoring measurements showed that the effect was significantly worse for a receiver far away from the nearest network reference station.

**Key Points:**
- Small space weather events can have a large local impact at high latitudes
- At high latitudes, warnings based on global indices are not as suitable
- The effects are amplified for users of a service with no receivers nearby

**Correspondence to:**
Y. L. Andalsvik,
andyng@kartverket.no

**Citation:**
Andalsvik, Y. L., and K. S. Jacobsen (2014), Observed high-latitude GNSS disturbances during a less-than-minor geomagnetic storm, *Radio Sci.*, *49*, 1277–1288, doi:10.1002/2014RS005418.

Received 5 MAR 2014
Accepted 28 NOV 2014
Accepted article online 2 DEC 2014
Published online 26 DEC 2014



## 1. Introduction

Space weather can severely affect Global Navigation Satellite Systems (GNSS) and augmentation systems (e.g., Ground Based Augmentation Systems and Satellite Based Augmentation Systems (SBAS)), causing degradation in the service. The disturbances are most severe in equatorial regions and at high latitudes. At high latitudes the disturbances are less regular and more dependent on geomagnetic storms than at equatorial latitudes and thus harder to predict [*Basu et al.*, 2002].

Norway is situated at latitudes such that under quiet conditions the auroral oval is typically located over the northernmost part of Norway. For more active days, however, the auroral oval will move southward to the middle and even southern parts of Norway. This location makes it ideal to study space weather effects on high latitudes.

The interaction of the solar wind with the magnetic field and atmosphere of the Earth causes, among other effects, disturbances in the ionosphere. As satellite signals from GNSS pass through the ionosphere, they are refracted and diffracted by these disturbances. The resulting rapid variations of signal amplitude and phase that are observed by a receiver on the ground may cause loss of lock or cycle slips. Even if none of those effects occur, it will increase the noise of the phase measurements. The strength of the amplitude and phase variations is commonly quantified using the scintillation indices $S_4$ and $\sigma_\phi$, which will be discussed in later sections. General overviews on the topic of space weather are found in *Eastwood* [2008] and *Singh et al.* [2010].

The occurrence of scintillation at high latitudes is related to the auroral oval, cusp, and polar cap patches, through the formation of small-scale plasma structures due to particle precipitation or plasma instabilities [e.g., *Aarons*, 1997; *Kersley et al.*, 1995; *Krankowski et al.*, 2006; *Weber et al.*, 1986; *Skone et al.*, 2009; *Tiwari et al.*, 2010; *Aquino et al.*, 2005; *Kivanc and Heelis*, 1997; *Burston et al.*, 2010; *Spogli et al.*, 2009; *Prikryl et al.*, 2013; *Smith et al.*, 2008]. It has been observed that phase scintillation occurs more often than amplitude scintillation at high latitudes and that scintillation is more common on geomagnetically disturbed days in the auroral oval region and close to noon and midnight [e.g., *Tiwari et al.*, 2010; *Jiao et al.*, 2013]. The level of disturbances and the shape and location of the auroral oval are not fixed. Generally, with increasing levels of geomagnetic activity, the auroral oval will expand toward the equator. Thus, the range of latitudes affected will depend on the level of activity. Scintillation activity has been observed at high latitudes for low *Kp* ($\lesssim 4$) [e.g., *Rodrigues et al.*, 2004; *Prikryl et al.*, 2010]. This is as expected, as the auroral oval is located at high latitudes during quiet conditions. For moderately active geomagnetic conditions ($Kp \approx 4$), there may be some ionospheric disturbances in the auroral zone, but the auroral oval will not expand significantly. An overview of recent research on the space weather processes in the polar cap is found in *Moen et al.* [2013].

The impact of scintillation is to some extent dependent on the receiver hardware. Some receivers are able to track a signal down to a lower amplitude than other receivers, and some receivers tolerate a greater

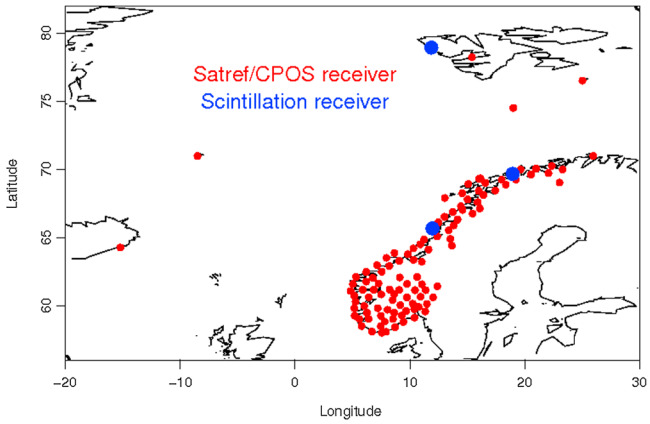


**Figure 1.** Scintillation receivers in operation at the time of the event (blue) and NMA GNSS reference stations (red).

variation in signal phase before a cycle slip or loss of lock occurs. However, no hardware can eliminate the phase noise. The impact of cycle slips, loss of lock, and noise will be dependent on the data processing scheme, but some general effects will be common to all processing:

1. Loss of lock will lead to a loss of results.
2. Uncorrected cycle slips will lead to full or partial resets of time series and data assimilation filters, or very large errors if such filters are not reset.
3. Increased phase noise will lead to increased noise in the results.

Some case studies on the impact of scintillation on GNSS receiver hardware are found in the papers by *Sreeja et al.* [2011, 2012] and *Strangeways et al.* [2011]. A review of the effects of ionospheric scintillations on the GPS system is found in *Kintner et al.* [2007]. Ultimately, the disturbed GNSS measurements lead to a degradation of the positioning accuracy [e.g., *Aquino et al.*, 2007; *Afraimovich et al.*, 2009; *Tiwari et al.*, 2009; *Moreno et al.*, 2011].

Most published case studies focus on major events. This paper, however, focuses on a case study of a minor geomagnetic event, which did not even reach storm level on the NOAA scale [*Poppe*, 2000]. According to the NOAA scale, the minor geomagnetic storm level G1 is defined to be reached at a *Kp* equal to 5. In the "Space Weather Scales" table in *Poppe* [2000], the first mention of satellite navigation problems ("...intermittent satellite navigation and low-frequency radio navigation problems may occur, ...") is at the strong geomagnetic storm level G3, which corresponds to a *Kp* equal to 7. For the event studied in this paper, *Kp* reached a maximum of 4.

In section 2, the data sources are presented. The observations are presented in section 3 and discussed in section 4. Section 5 contains the conclusions of this case study.

## 2. Data Sources

### 2.1. NMA Receiver Network

The Norwegian Mapping Authority (NMA) operates a nationwide network of 1 Hz geodetic receivers with a typical interstation distance of around 50–60 km.

In addition NMA, at the time of this event, operated three scintillation monitoring receivers capable of collecting raw observation data at 100 Hz. Two of them are owned by CNES (Centre National d'Études Spatiales). These receivers were all Septentrio PolaRxS receivers, located in Ny-Ålesund (Latitude: 78.5°N, Longitude: 11.9°E), Tromsø (Latitude: 70°N, Longitude: 18.9°E), and Vega (Latitude: 66.1°N, Longitude: 12.0°E). The location of the receivers described in this subsection is shown in Figure 1.

### 2.2. The Positioning Service "CPOS"

NMA provides a nationwide network real-time kinematic (NRTK) positioning service, based on data from the NMA receiver network.

This service is named CPOS, offering real-time positioning at centimeter level accuracy for users in Norway. At the time of the event, the RTK service was supplied using the GPSNet software from Trimble. CPOS uses

dual-frequency measurements from the GPS and GLONASS satellites. The maximum separation between adjacent stations is 70 km, while a typical interstation distance is around 50–60 km.

Some more information regarding CPOS can be found in *Jacobsen and Schäfer* [2012].

### 2.3. Real-Time Ionospheric Monitor

The Real-Time Ionospheric Monitor (RTIM) software also receives the real-time data stream from the NMA receiver network, from which it computes various measures of the state of the ionosphere, including the Vertical Total Electron Content (VTEC) and the Rate of TEC Index (ROTI).

More detailed descriptions of RTIM, VTEC, and ROTI can be found in *Jacobsen and Schäfer* [2012].

### 2.4. Real-Time Ionosphere Scintillation Monitor

The scintillation indices $S_4$ and $\sigma_\phi$ are calculated in real time at each scintillation receiver site using our own software, Real-Time Ionosphere Scintillation (RTIS). The indices are then sent every minute to the NMA facilities at Hønefoss.

#### 2.4.1. Phase Scintillations

$\sigma_\phi$ is the widely used index to characterize phase scintillation activity. It is defined as the standard deviation of the detrended carrier phase.

$$\sigma_\phi = \sqrt{\langle \phi^2 \rangle - \langle \phi \rangle^2}$$

Before calculating the standard deviation, the raw phase measurements are filtered using a sixth-order high-pass digital Butterworth filter as seen in, e.g., *Van Dierendonck et al.* [1993]. The cutoff frequency used is 0.3 Hz, as proposed by *Forte* [2005], which is higher than the standard value of 0.1 Hz that is more appropriate for equatorial regions.

To avoid the edge effects of the filtering process, the interval of data that is passed to the filter is longer than the time interval used for the final calculation of the scintillation index. The software internally keeps a continuously updated record of the previous 240 s of data. Each minute, the current data are passed to the filtering process. The standard deviation is calculated using a 1 min interval between $t = 120$ s and $t = 180$ s. In this way the $\sigma_\phi$ index is calculated each minute, based on 1 min of data, without any numerical artifacts from the filtering process.

#### 2.4.2. Amplitude Scintillations

The amplitude scintillations is characterized by the $S_4$ index that is defined as the ratio of the standard deviation of the signal power to the mean signal power. The total $S_4$, including ambient noise effects, is

$$S_{4\text{tot}} = \sqrt{\frac{\langle I^2 \rangle - \langle I \rangle^2}{\langle I \rangle^2}} \tag{1}$$

where $\langle\rangle$ denotes the average over 60 s of the quantity inside the brackets. The intensity measurements are detrended by filtering the original intensity measurements with a sixth-order low-pass Butterworth filter and then dividing the original signal by the detrended signal

$$I(t) = \frac{I_{\text{orig}}(t)}{I_{\text{filtered}}(t)} \tag{2}$$

where $I$ is the signal intensity [*Van Dierendonck et al.*, 1993]. The part of the $S_4$ value that is due to ambient noise can be written

$$S_{4\text{corr}} = \sqrt{\frac{100}{S/N_0}\left[1 + \frac{500}{19S/N_0}\right]} \tag{3}$$

If a 60 s estimate of the signal-to-noise density, $S/N_0$, is then used, this correction can then be subtracted to get the $S_4$ value without the noise effects

$$S_4 = \sqrt{S_{4\text{tot}}^2 - S_{4\text{corr}}^2} \tag{4}$$

If the argument under the square root becomes negative, it is set to zero [*International Civil Aviation Organization (ICAO)*, 2006].

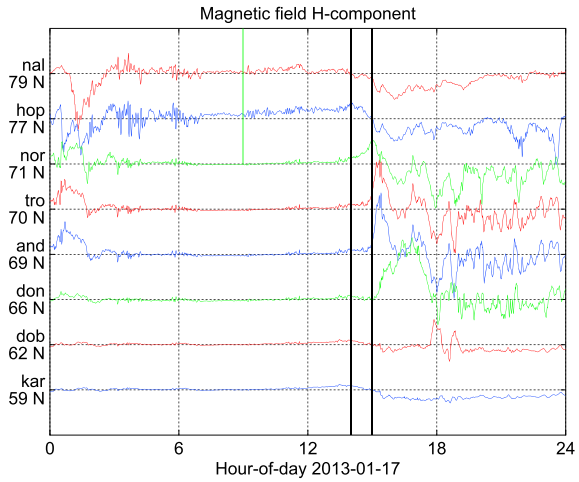


**Figure 2.** Magnetometer data from the Norwegian chain. The stations are sorted by latitude and are as follows: (from top to bottom) Ny-Ålesund (nal), Hopen(hop), Nordkapp (nor), Tromsø(tro), Andøya (and), Dønna (don), Dombås (dob), and Karmøy (kar). Vertical black lines have been added at 14 and 15 UT. For each magnetometer, a line is plotted showing the deviation of the horizontal component from its median value. The dotted line for each magnetometer marks the zero line for that magnetometer, and the distance between the dotted lines is equal to 200 nT.

## 3. Observations

On 17 January 2013 a weak geomagnetic storm was observed in Norway. Magnetic disturbances were first observed around 14 UT by the northernmost magnetometers in the Norwegian magnetometer chain (see Figure 2). The magnetic disturbances expanded southward, rising sharply at magnetometers in northern and middle Norway around 15 UT and persisting for the rest of the day.

The 3 h planetary *Kp* index, however, only reached 4 (see Figure 3), which is below the NOAA scale of geomagnetic storms. Local geomagnetic disturbances has been shown to be well correlated to the occurrence of scintillation [e.g., *Tiwari et al.*, 2010; *Jiao et al.*, 2013]. The local geomagnetic disturbances can be quantified by the local *K* index, which is calculated from one magnetometer's measurements. Figure 4 shows the local *K* index for the locations Tromsø and Rørvik. Rørvik is approximately midway between the scintillation receiver at Vega and the GNSS monitor at Steinkjer. The local *K* indices show the same general features as the global *K* index, with low values at 06–12 UT and a peak at 15–18 UT. However, the local *K* indices are lower than the global during 06–12 UT and their peak at 15–18 UT is slightly higher, with a value of 5 instead of 4, indicating that the local geomagnetic activity is higher than the global level in the area investigated.

The geomagnetic storm was caused by the impact of a coronal mass ejection (CME) which had been launched by an M class solar flare on 13 January 2013. The CME reached Earth on 17 January, delivering a glancing blow to the magnetosphere.

### 3.1. Solar Wind Data

Solar wind interplanetary magnetic field (IMF) is shown in Figure 5, and solar wind velocity and pressure are shown in Figure 6.

The solar wind interplanetary magnetic field (IMF) increased in magnitude around 14 UT up to approximately 16 nT, while the $B_z$ component showed a rapid southward turning, dropping from 10 nT to −6 nT in 10 min. Between 14 and 15 UT, the IMF $B_z$ was stable and southward. Shortly after 15 UT, there is a brief increase in $B_z$. Following this there is a larger, but still brief, decrease between 15:45 and 16:00 UT. At 16:25 UT, $B_z$ rises to ≈ 0 nT and stays at that level for half an hour before dropping to −12 nT. After this, $B_z$ is stable and southward for several hours and then it gradually increases. At the end of the day, it has increased to almost −3 nT.

The pressure increased from a base level of 5 nPa at 10 UT, to an enhanced pressure of around 15 nPa for the time from 13:15 to 15:15 UT, with peaks slightly above 20 nPa. Shortly after 15 UT, the pressure rose from 15 nPa to 20 nPa in around 8 min, stayed at 20 nPa for a few minutes then fell from 20 to 5 nPa in just 5 min.

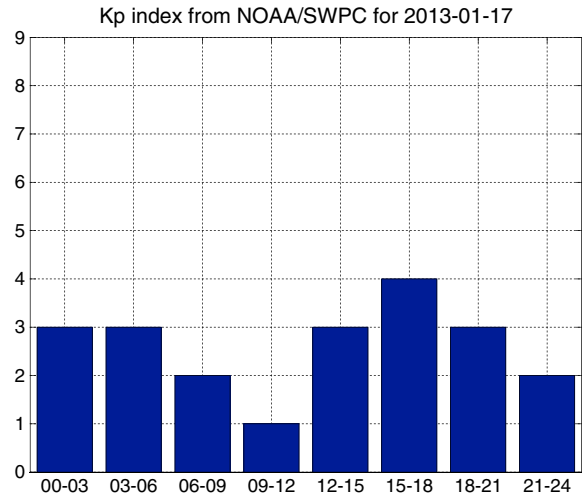


**Figure 3.** Three hour planetary *Kp* index for 17 January 2013.

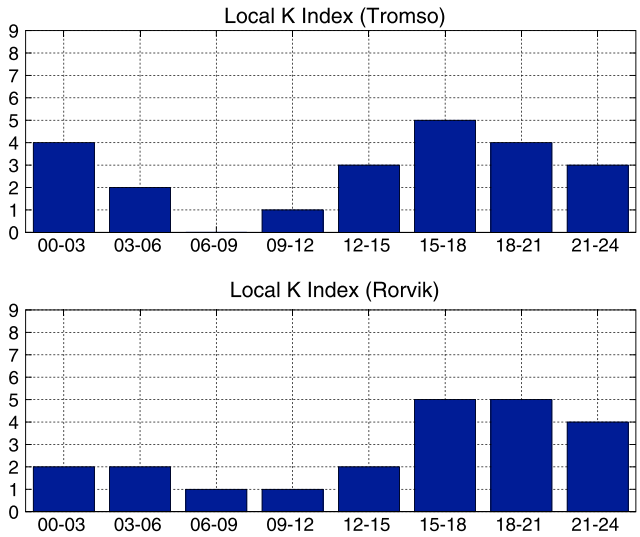


**Figure 4.** Three hour local *K* index for 17 January 2013, for the magnetometers at Tromsø and Rørvik.

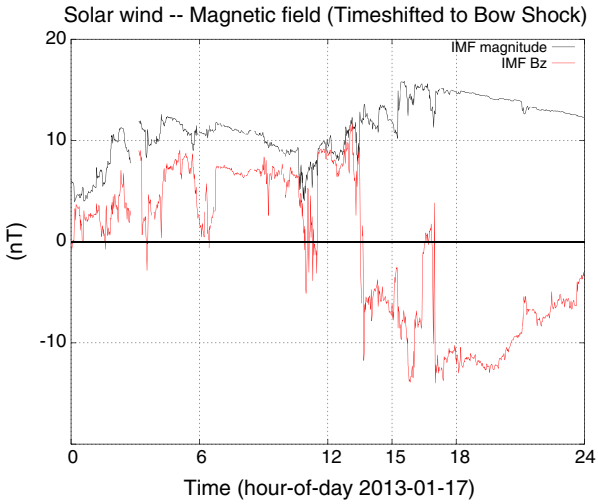


**Figure 5.** IMF $B_z$ component in red and $B_{tot}$ in black. The dashed line at 15 UT indicates the onset of the first geomagnetic activity.

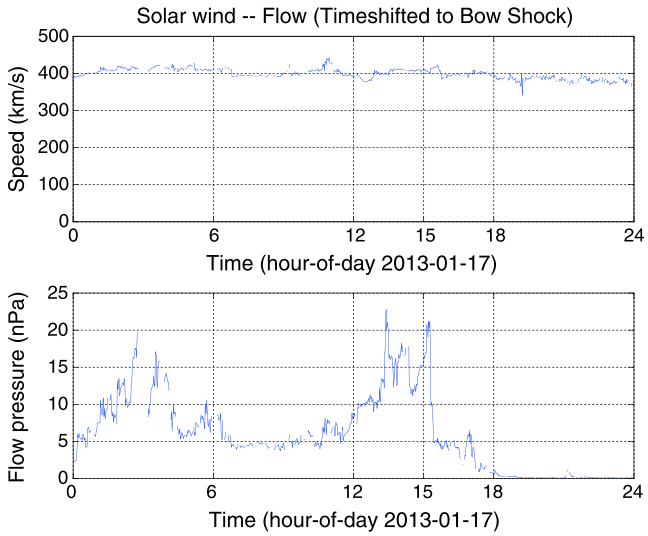


**Figure 6.** (top) Solar wind speed and (bottom) flow pressure for 17 January 2013.

After that, the pressure gradually decreased until it was at about 0.1 nPa and stayed at that level for the rest of the day. We note that between 0 and 6 UT, there was an increase and decrease of pressure caused by another plasma structure passing the Earth, but the magnetic field structure was not particularly interesting and it did not cause any major effects.

The solar wind velocity did not exhibit any significant variations.

### 3.2. ROTI

RTIM time series plots for ROTI (see Figure 7) shows a behavior similar to the magnetometer data at corresponding latitudes. The increase in activity starts around 15 UT and continues with a peak between 16 and 19 UT and a gradual decrease until the end of the day. The values are generally highest for the northern part of Norway (67°–72°), and lowest for the southern part of Norway (57°–62°).

### 3.3. Scintillations

The scintillation monitors show similar results. Results from two of the scintillation receivers operated by NMA, on Vega and in Tromsø, are shown in Figures 8 and 9, respectively. The indices increase from around 15 UT, and Tromsø, which is further north than Vega, reached a slightly higher scintillation level. The highest

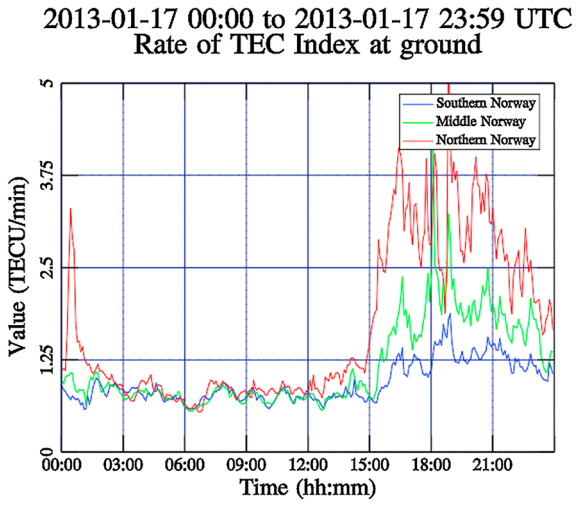


**Figure 7.** Time series of Rate of TEC Index (ROTI) at ground for Northern (red), Middle (green), and Southern (blue) Norway.

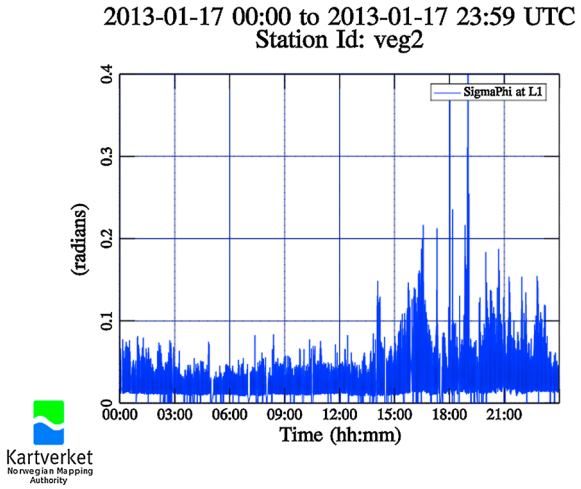


**Figure 8.** $\sigma_\Phi$ index for L1 from the Vega station. The plot shows data from all satellites in view.

peak for phase scintillations on GPS L1 for the Tromsø receiver was at 0.569 radians followed by three other peaks exceeding 0.4, which corresponds to a moderate level of scintillation.

*Jiao et al.* [2013] found a good correlation between the phase and amplitude scintillation indices and the geomagnetic field disturbances which seems to correspond with the data found for this case.

### 3.4. CPOS Network Disruptions

Figures 10 and 11 show network disruptions for northern and middle Norway, respectively. Disruptions are measured as the percentage of stations for which less than 10% of the satellites in view can be used by the RTK software. The stations in middle Norway show small disruptions, while the stations in northern Norway were strongly disrupted for several hours.

Figures 12 and 13 show position noise (top) and position bias (bottom) for Tromsø and Steinkjer, respectively. The position noise is the standard deviation of the offset between the measured height and the true height, where the true height is defined as the median height. The bias is the mean of the offset. The noise and bias were calculated for 60 s intervals.

### 3.5. EGNOS Performance

Ionospheric disturbances can also cause reduced performance of satellite-based augmentation (SBAS) systems. The European SBAS system is the European Geostationary Overlay System (EGNOS). The EGNOS corrections are computed based on data from the Ranging Integrity Monitoring Stations (RIMS) network.

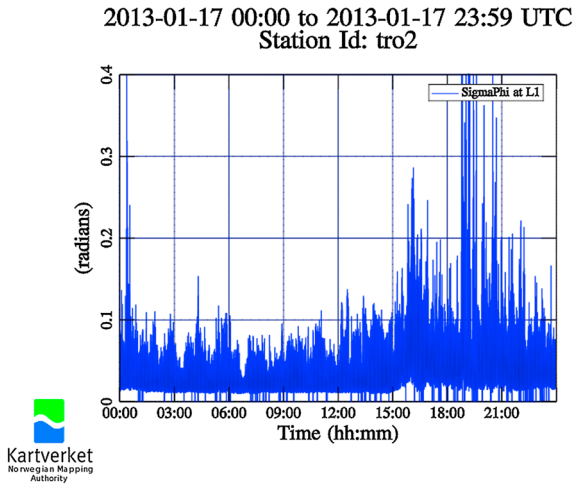


**Figure 9.** $\sigma_\Phi$ index for L1 from the Tromsø station. The plot shows data from all satellites in view.

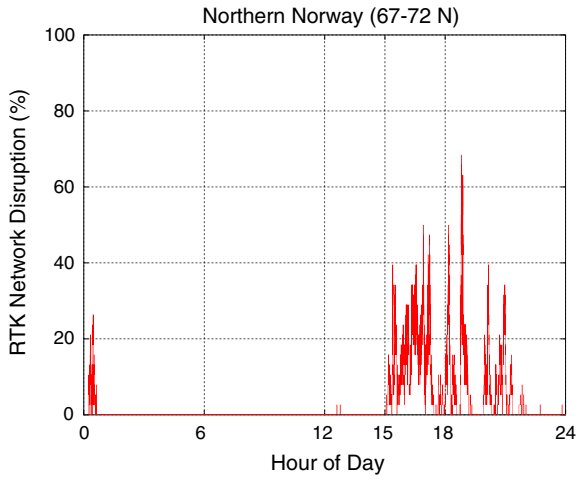


**Figure 10.** NRTK network disruptions in Northern Norway.

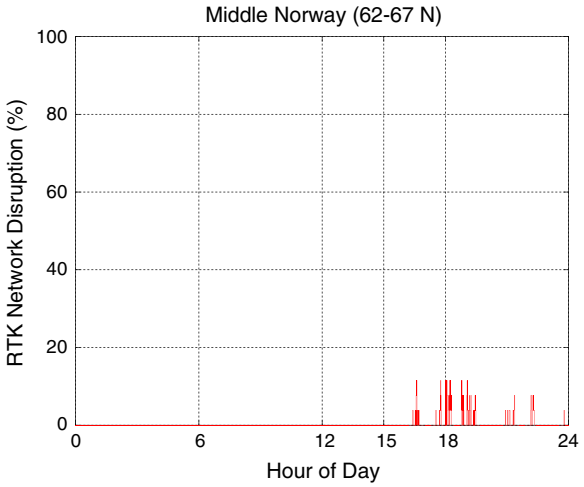


**Figure 11.** NRTK network disruptions in Middle Norway.

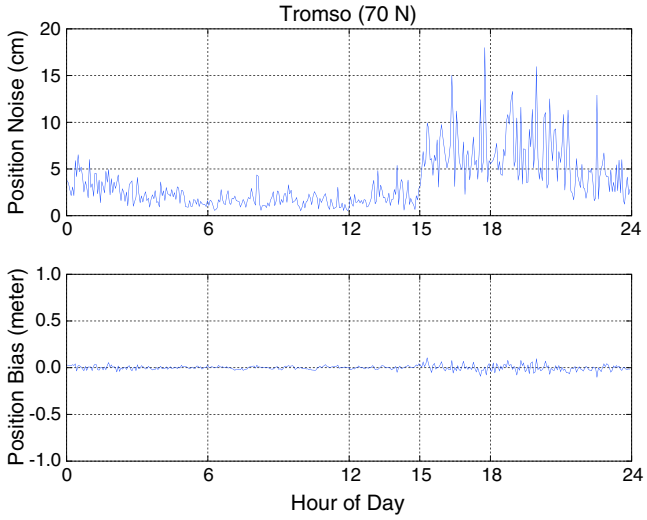


**Figure 12.** Position (top) noise and (bottom) bias at Tromsø in Northern Norway.

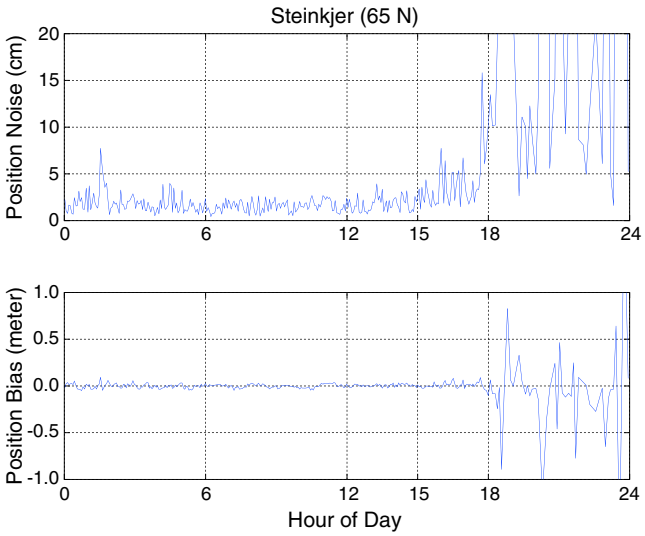


**Figure 13.** Position (top) noise and (bottom) bias at Steinkjer in Middle Norway.

Figures 14 and 15 show availability for when the Approach with Vertical Guidance (APV1) integrity and continuity requirements are met for EGNOS for 16 and 17 January. The EGNOS availability is calculated as the percentage of the time the vertical protection level and horizontal protection level is below the horizontal and vertical alarm limits. The availability must be over 99% according to the International Civil Aviation Organization [*ICAO*, 2006]. The EGNOS performance is influenced by, among other factors, ionospheric disturbances.

Comparing the 2 days, a reduction in availability is seen on 17 January for Iceland, northern Norway, and northern Finland.

This corresponds well with the areas affected by the geomagnetic activity. The reduction is not as large as for some events, but it is a noticeable reduction of the area with 99% availability in northern Norway. All of the RIMS were functioning at the time, so the reduction in availability could not have been a result of lack of data from a station.

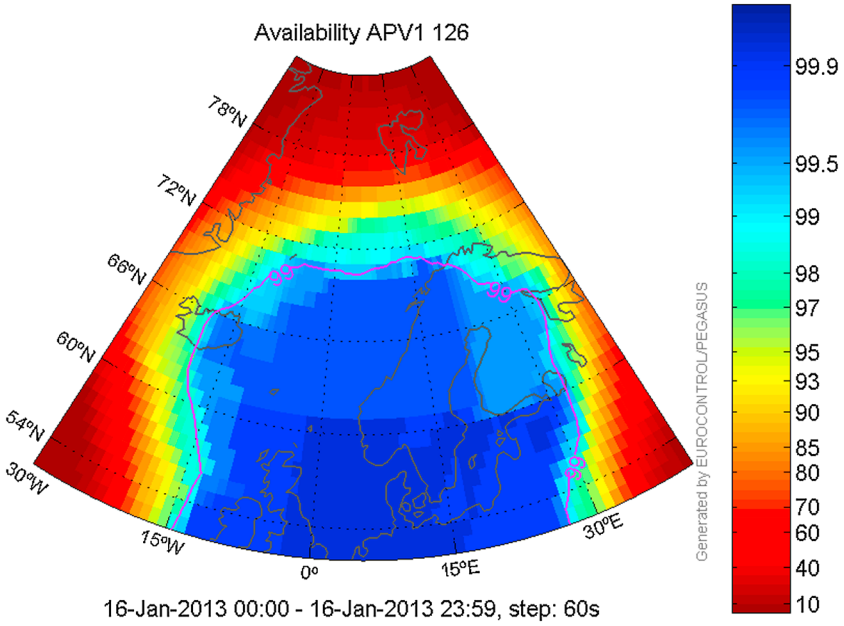


**Figure 14.** EGNOS APV1 availability on 16 January 2013. The purple line shows the 99% availability limit.

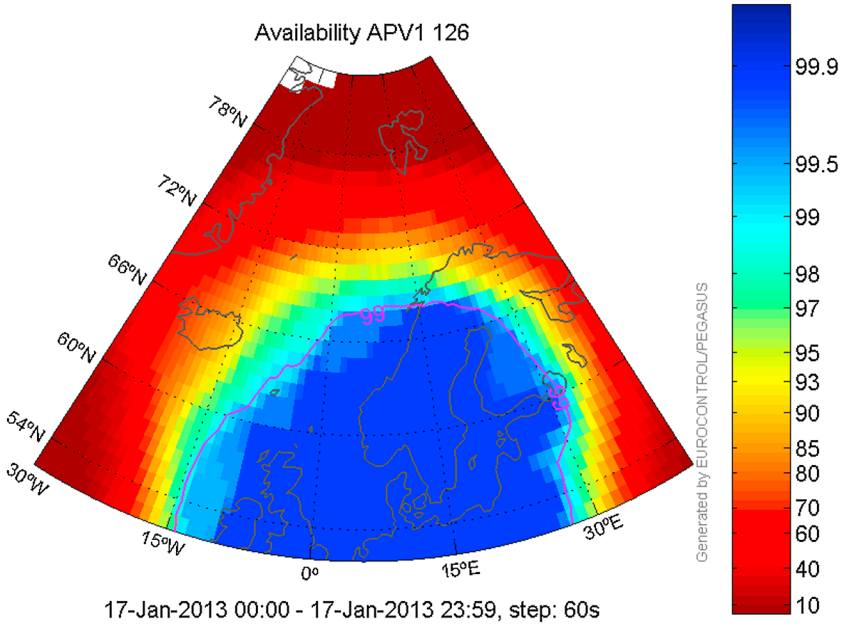


**Figure 15.** APV1 availability on 17 January 2013. The purple line shows the 99% availability limit.

## 4. Discussion

On 17 January 2013 a CME impacted the Earth's magnetosphere (see Figures 5 and 6). The most commonly used measure of global magnetic disturbance, the *Kp* index, increased to 4 (see Figure 3), which is below the NOAA scale of geomagnetic storms. Based on that alone, this event could be considered a nonevent, and in most geographic locations this would be the case. Local *K* indices provided a more appropriate indication of the disturbances in the ionosphere, indicating greater disturbances during the time interval of GNSS disruptions. However, the description of impacts given in *Poppe* [2000] for a *Kp* level of 5 does not indicate that there should be any problem for satellite navigation. A separate table, similar to the table in *Poppe* [2000], may be required to provide accurate descriptions of impacts as a function of local *K* indices at high latitudes.

At high latitudes, however, significant disturbances were recorded by magnetometer and GNSS observations (see Figures 2 and 7–9). Some precursor activity was seen from 14 UT, particularly at the highest latitude magnetometers. Then, at 15 UT, activity suddenly and rapidly increased. The disturbances, measured by ROTI and $\sigma_\phi$, were more intense in the northern parts of Norway than in the middle and southern parts.

The network RTK service CPOS experienced difficulties in processing the recorded measurements, resulting in loss of usable satellites. That is, no correction could be computed for those satellites, and as such they could not be used by the users of the service. This effect strongly affected the northern Norway network (see Figure 10). The network in middle Norway was only lightly affected by this effect (see Figure 11). The end effect of the ionospheric disturbances for the users of the service was measured by GNSS monitors in northern and middle Norway (see Figures 12 and 13). Both monitors recorded higher noise levels in the calculated heights, but the monitor in middle Norway also recorded significant biases, on the order of 1 m, in the height. The fact that the GNSS monitor in middle Norway, which experienced less noise, scintillation, and network disruption, had the most severe errors can be explained by the fact that it was located far from the nearest network reference station. In addition to the increased noise, the ionosphere becomes less homogeneous during space weather activity, due to particle precipitation and plasma convection. This decreases the range at which the interpolated correction values from the network RTK is valid.

Finally, we have included two overview plots of EGNOS APV1 availability (see Figures 14 and 15), showing that the EGNOS service also experienced a reduced availability at high latitudes due to this space weather event. Figure 14 shows the status for 16 January, which was a quiet day. Figure 15 shows the status on the

day of the event, for which there was clearly a reduction in availability in northern Norway and Finland and on Iceland.

The effects of space weather are not equally distributed over the Earth. At high latitudes, the most important feature related to space weather is the auroral oval. The auroral oval is a footprint of the large-scale structures in the magnetosphere. Plasma structures in the solar wind interacts with the magnetosphere, transferring energy and particles from the solar wind to the magnetosphere. Under certain conditions, these may be stored in the magnetosphere for a while and then released. This is known as a substorm [*Eastwood*, 2008; *Akasofu*, 1964]. The impact of a substorm is felt in the auroral oval region. This case study shows the impact of such an event.

Solar wind data was presented in section 3.1. Between 14 and 15 UT, the IMF $B_z$ was stable and southward. During stable, southward IMF $B_z$, energy is transferred from the solar wind and stored in the magnetosphere [*Eastwood*, 2008]. Just after 15 UT a sharp and short-lived increase in IMF $B_z$, along with a rapid change in pressure, might have triggered the release of that energy. The space weather conditions were not severe enough to significantly expand the auroral oval and create a global geomagnetic storm. However, it caused disturbances at high latitudes, in the region where the auroral oval is located during normal activity levels. This is an example of a space weather effect that may occur at high latitudes, while lower latitudes do not suffer detrimental effects.

## 5. Conclusions

This paper presented a case study of a space weather event that occurred on 17 January 2013, focusing on the effects on a network RTK positioning service. This section contains the main conclusions of this paper.

1. Weak space weather events can have a large local impact at high latitudes. Warnings based on global indices such as *Kp* are not suitable, or should at least be interpreted differently, by users at high latitudes.
2. Local *K* indices provide a better indication of the level of activity, but the table in *Poppe* [2000] that describes impacts as a function of *K* index may not be directly applicable to users at high latitudes. A significant effort would be required to collect information to make a similar table linking local *K* indices to impacts for users at high latitudes.
3. The effects are amplified for users that receive corrections from a support network which has no reference stations close to the user (presumably because of a decreased spatial correlation distance in the ionosphere).

**Acknowledgments**
The *Kp* index data were downloaded from NOAA/SWPC. Two of the scintillation receivers are operated in collaboration with CNES. We thank Magnar G. Johnsen at Tromsø Geophysical Observatory at UiT the Arctic University of Norway for providing the magnetometer data. Solar wind data (IMF, speed, and pressure) were downloaded from the OMNIWeb webpage of NASA/GSFC.

## References

Aarons, J. (1997), Global positioning system phase fluctuations at auroral latitudes, *J. Geophys. Res.*, *102*(A8), 17,219–17,231, doi:10.1029/97JA01118.

Afraimovich, E., E. Astafyeva, V. Demyanov, and I. Gamayunov (2009), Mid-latitude amplitude scintillation of GPS signals and GPS performance slips, *Adv. Space Res.*, *43*, 964–972, doi:10.1016/j.asr.2008.09.015.

Akasofu, S.-I. (1964), The development of the auroral substorm, *Planet. Space Sci.*, *12*, 273–282.

Aquino, M., F. S. Rodrigues, J. Souter, T. Moore, A. Dodson, and S. Waugh (2005), Ionospheric scintillation and impact on GNSS users in northern Europe: Results of a 3 year study, *Space Commun.*, *20*(1–2), 17–29.

Aquino, M., A. Dodson, J. Souter, and T. Moore (2007), Ionospheric scintillation effects on GPS carrier phase positioning accuracy at auroral and sub-auroral latitudes, in *Dynamic Planet, International Association of Geodesy Symposia*, vol. 130, edited by M. Aquino et al., pp. 859–866, Springer, Berlin, doi:10.1007/978-3-540-49350-1_121.

Basu, S., K. Groves, S. Basu, and P. Sultan (2002), Specification and forecasting of scintillations in communication/navigation links: Current status and future plans, *J. Atmos. Sol. Terr. Phys.*, *64*(16), 1745–1754, doi:10.1016/S1364-6826(02)00124-4.

Burston, R., I. Astin, C. Mitchell, L. Alfonsi, T. Pedersen, and S. Skone (2010), Turbulent times in the northern Polar ionosphere?, *J. Geophys. Res.*, *115*(A4), A04310, doi:10.1029/2009JA014813.

Eastwood, J. P. (2008), The science of space weather, *Philos. Trans. R. Soc. A*, *366*(1884), 4489–4500, doi:10.1098/rsta.2008.0161.

Forte, B. (2005), Optimum detrending of raw GPS data for scintillation measurements at auroral latitudes, *J. Atmos. Sol. Terr. Phys.*, *67*(12), 1100–1109, doi:10.1016/j.jastp.2005.01.011.

International Civil Aviation Organization (ICAO) (2006), *Standards and Recommended Practices*. Radio Navigation Aid, 1.

Jacobsen, K. S., and S. Schäfer (2012), Observed effects of a geomagnetic storm on an RTK positioning network at high latitudes, *J. Space Weather Space Clim.*, *2*, A13, doi:10.1051/swsc/2012013.

Jiao, Y., Y. T. Morton, S. Taylor, and W. Pelgrum (2013), Characterization of high-latitude ionospheric scintillation of GPS signals, *Radio Sci.*, *48*, 698–708, doi:10.1002/2013RS005259.

Kersley, L., C. D. Russell, and D. L. Rice (1995), Phase scintillation and irregularities in the northern Polar ionosphere, *Radio Sci.*, *30*(3), 619–629, doi:10.1029/94RS03175.

Kintner, P. M., B. M. Ledvina, and E. R. de Paula (2007), GPS and ionospheric scintillations, *Space Weather*, *5*, S09003, doi:10.1029/2006SW000260.

Kivanc, Ö., and R. A. Heelis (1997), Structures in ionospheric number density and velocity associated with polar cap ionization patches, *J. Geophys. Res.*, *102*(A1), 307–318, doi:10.1029/96JA03141.

Krankowski, A., I. Shagimuratov, L. Baran, I. Ephishov, and N. Tepenitzyna (2006), The occurrence of polar cap patches in TEC fluctuations detected using GPS measurements in southern hemisphere, *Adv. Space Res.*, *38*(11), 2601–2609, doi:10.1016/j.asr.2005.12.006, middle and Upper Atmospheres, Active Experiments, and Dusty Plasmas.

Moen, J., K. Oksavik, L. Alfonsi, Y. Daabakk, V. Romano, and L. Spogli (2013), Space weather challenges of the polar cap ionosphere, *J. Space Weather Space Clim.*, *3*, A02, doi:10.1051/swsc/2013025.

Moreno, B., S. Radicella, M. C. Lacy, M. Herraiz, and G. Rodriguez-Caderot (2011), On the effects of the ionospheric disturbances on precise point positioning at equatorial latitudes, *GPS Solutions*, *15*(4), 381–390, doi:10.1007/s10291-010-0197-1.

Poppe, B. B. (2000), New scales help public, technicians understand space weather, *Eos Trans. AGU*, *81*(29), 322–328, doi:10.1029/00EO00247.

Prikryl, P., P. T. Jayachandran, S. C. Mushini, D. Pokhotelov, J. W. MacDougall, E. Donovan, E. Spanswick, and J.-P. St.-Maurice (2010), GPS TEC, scintillation and cycle slips observed at high latitudes during solar minimum, *Ann. Geophys.*, *28*(6), 1307–1316, doi:10.5194/angeo-28-1307-2010.

Prikryl, P., R. Ghoddousi-Fard, B. S. R. Kunduri, E. G. Thomas, A. J. Coster, P. T. Jayachandran, E. Spanswick, and D. W. Danskin (2013), GPS phase scintillation and proxy index at high latitudes during a moderate geomagnetic storm, *Ann. Geophys.*, *31*(5), 805–816, doi:10.5194/angeo-31-805-2013.

Rodrigues, F. S., M. H. O. Aquino, A. Dodson, T. Moore, and S. Waugh (2004), Statistical analysis of GPS ionospheric scintillation and short-time TEC variations over northern Europe, *Navigation*, *51*(1), 59–75, doi:10.1002/j.2161-4296.2004.tb00341.x.

Singh, A. K., D. Singh, and R. P. Singh (2010), Space weather: Physics, effects and predictability, *Surv. Geophys.*, *31*, 581–638, doi:10.1007/s10712-010-9103-1.

Skone, S., M. Feng, R. Tiwari, and A. Coster (2009), Characterizing ionospheric irregularities for auroral scintillations, paper presented at 22nd International Technical Meeting of the Satellite Division of the Institute of Navigation (ION GNSS 2009), pp. 2551–2558, Savannah, Ga, Sept.

Smith, A. M., C. N. Mitchell, R. J. Watson, R. W. Meggs, P. M. Kintner, K. Kauristie, and F. Honary (2008), GPS scintillation in the high arctic associated with an auroral ARC, *Space Weather*, *6*, S03D01, doi:10.1029/2007SW000349.

Spogli, L., L. Alfonsi, G. De Franceschi, V. Romano, M. H. O. Aquino, and A. Dodson (2009), Climatology of GPS ionospheric scintillations over high and mid-latitude European regions, *Ann. Geophys.*, *27*(9), 3429–3437, doi:10.5194/angeo-27-3429-2009.

Sreeja, V., M. Aquino, and Z. G. Elmas (2011), Impact of ionospheric scintillation on GNSS receiver tracking performance over Latin America: Introducing the concept of tracking jitter variance maps, *Space Weather*, *9*, S10002, doi:10.1029/2011SW000707.

Sreeja, V., M. Aquino, Z. G. Elmas, and B. Forte (2012), Correlation analysis between ionospheric scintillation levels and receiver tracking performance, *Space Weather*, *10*, S06005, doi:10.1029/2012SW000769.

Strangeways, H. J., Y. Ho, M. H. O. Aquino, Z. G. Elmas, H. A. Marques, J. F. G. Monico, and H. A. Silva (2011), On determining spectral parameters, tracking jitter, and GPS positioning improvement by scintillation mitigation, *Radio Sci.*, *46*, RS0D15, doi:10.1029/2010RS004575.

Tiwari, R., S. Bhattacharya, P. K. Purohit, and A. K. Gwal (2009), Effect of TEC variation on GPS precise point at low latitude, *Open Atmos. Sci. J.*, *3*, 1–12, doi:10.2174/1874282300903010001.

Tiwari, R., F. Ghafoori, O. Al-Fanek, O. Haddad, and S. Skone (2010), Investigation of high latitude ionospheric scintillations observed in the Canadian region, paper presented at 23rd International Technical Meeting of the Satellite Division of the Institute of Navigation (ION GNSS 2010), pp. 349–360, Portland, Oreg., Sept.

Van Dierendonck, A. J., J. Klobuchar, and Q. Hua (1993), Ionospheric scintillation monitoring using commercial single frequency C/A code receivers, 6th International Technical Meeting of the Satellite Division of the Institute of Navigation (ION GPS 1993), pp. 1333–1342, Salt Lake City, Utah, Sept.

Weber, E. J., J. A. Klobuchar, J. Buchau, H. C. Carlson, R. C. Livingston, O. de la Beaujardiere, M. McCready, J. G. Moore, and G. J. Bishop (1986), Polar cap *F* layer patches: Structure and dynamics, *J. Geophys. Res.*, *91*(A11), 12,121–12,129, doi:10.1029/JA091iA11p12121.